JOURNAL OF MAGNETIC RESONANCE **129,** 115–124 (1997)
ARTICLE NO. MN971263

Design of Selective Adiabatic Inversion Pulses Using the Adiabatic Condition

Daniel Rosenfeld,*,[1] Shimon L. Panfil,† and Yuval Zur†

*School of Physics and Astronomy, Tel-Aviv University, Tel Aviv 69978, Israel; and †Elscint MRI Center, POB 550, Haifa 31004, Israel

Received May 19, 1997; revised August 20, 1997

Adiabatic RF pulses play an important role in spin inversion due to their robust behavior in the presence of inhomogeneous RF fields. These pulses are characterized by the trajectory swept by the tip of the B_{eff} vector and the rate of motion along it. In this paper, we describe a method by which optimized modulation functions can be constructed to render insensitivity to B_1 inhomogeneity over a predetermined B_1 range and over a wide band of frequencies. This is accomplished by requiring that the optimized pulse fulfill the adiabatic condition over this range of B_1 inhomogeneity and over the desired frequency band for the complete duration of the pulse. A trajectory similar to the well-known sech/tanh adiabatic pulse, i.e., a half-ellipse, is used. The optimization process improves the slice profile by optimizing the rate of motion along this trajectory. The optimized pulse can be tailored to the specific design requirements; in particular, the transition sharpness may be traded off against the inverted bandwidth. Two design examples, including experimental results, demonstrate the superiority of the optimized pulses over the conventional sech/tanh pulse: in the first example, a large frequency band is to be inverted using a weak RF amplitude in a short time. In the second example, a pulse with a very sharp transition is required.

INTRODUCTION

Adiabatic fast passage has long been used to invert a selected band of spins. These pulses retain their robustness even when subjected to nonuniform RF amplitude. The pulse is defined by its instantaneous amplitude $\omega_1(t) = \gamma B_1(t)$ and frequency $\omega(t)$ and is most conveniently studied in the *frequency frame* which is a frame of reference rotating at the instantaneous frequency of the pulse (*1*). It operates by causing the magnetization vector **m** to follow the effective field vector $\boldsymbol{\omega}_e$,

$$\boldsymbol{\omega}_e(\omega_0, t) = v\omega_1(t)\hat{\mathbf{x}} + \Delta\omega(\omega_0, t)\hat{\mathbf{z}}, \qquad [1]$$

where $\Delta\omega(\omega_0, t) = \omega(t) - \omega_0$ is the resonance offset and ω_0 the Larmor frequency of the spin we are inspecting. v is the RF field inhomogeneity factor with a nominal value of 1. The *adiabatic theorem* (*2*) asserts that the magnetization vector **m** remains spin-locked to $\boldsymbol{\omega}_e$ provided that the rate of precession of **m** about $\boldsymbol{\omega}_e$ is much faster than the angular velocity of the motion of $\boldsymbol{\omega}_e$. Mathematically this is expressed by the *adiabatic condition* (*3*),

$$\Gamma(\omega_0, t) \gg 1, \qquad [2]$$

where Γ is the adiabatic parameter,

$$\Gamma(\omega_0, t) = \frac{\|\boldsymbol{\omega}_e(\omega_0, t)\|}{|\dot{\theta}(\omega_0, t)|} = \frac{(v^2\omega_1^2 + \Delta\omega^2)^{3/2}}{v|\Delta\omega\dot{\omega}_1 - \omega_1\Delta\dot{\omega}|}, \qquad [3]$$

and $\tan\theta = \Delta\omega/\omega_1$. Inversion is obtained when the effective field moves the longitudinal magnetization M_z from the $+z$ to the $-z$ axis over a wide band of Larmor frequencies.

In the frame of reference of the slice center, i.e., for $\omega_0 = \omega_c$, we may plot the route traced by the tip of the $\boldsymbol{\omega}_e$ vector. This graph of $\omega_1(t)$ vs $\Delta\omega(\omega_c, t)$ is called the *trajectory* of the adiabatic pulse. An adiabatic pulse is characterized by its trajectory and the rate of motion of $\boldsymbol{\omega}_e$ upon it. When the adiabatic condition is strictly fulfilled, this trajectory is a good prediction of the route traced by the magnetization vector since the latter is ''locked'' to $\boldsymbol{\omega}_e$. However, at off resonances where the adiabatic condition collapses, such as in the transition region, the trajectory does not portray the path followed by the magnetization. Three classic examples of frequency modulation functions that have been analyzed (expressed here as amplitude/frequency modulation functions) include the sech/tanh (*4*), sin/cos (*5*), and const/tan (*3*).

[1] To whom correspondence should be addressed at Elscint MRI Center, POB 550, Haifa 31004, Israel. Fax: 972-4-8575-593. E-mail: danny@mri.elscint.co.il.

1090-7807/97 $25.00

A numerical optimization method called NOM (numerically optimized modulation) was introduced by Ugurbil *et al.* (*6*) and further generalized by Town and Rosenfeld (*7*) and Skinner and Robitaille (*8*). According to these methods the time variable t is parameterized by a function $\eta(t)$. Using Eq. [3], the purpose is to find the function $\eta(t)$ which results in a pulse with an adiabatic parameter which is equal to a desired value γ_0 during the entire duration of the pulse and over a given range of inhomogeneity ($v_{\min} \le v \le v_{\max}$). This may be done numerically (*6*) and in certain cases an analytic solution can be obtained (*7, 8*). The optimization, which turns out to use even less RF power than the original pulse, is effective only at the Larmor frequency of the slice center (on resonance) and is, therefore, inadequate for inversion of a large frequency bandwidth. Johnson *et al.* (*9*) subsequently extended this method to account for off-resonance conditions.

Several researchers (*10–13*) have recently suggested an analytic solution to this problem by equating Γ to a constant, $\Gamma(\omega_0, t) = \gamma_0$, for $\Delta\omega = 0$. It was assumed that the adiabatic parameter achieves its smallest and hence most critical value at the resonance Larmor frequency, where $\omega_0 = \omega(t)$.

In this paper NOM is generalized to include wide-band RF pulses which are suitable for MR imaging as well as spectroscopic applications. We require that the *minimal* value of Γ within the inverted band be equal to the constant γ_0. As is shown, this value is not obtained at the resonance isochromat $\omega_0 = \omega(t)$ but rather at some other Larmor frequency. The method presented enables the pulse designer to determine the trade-off of various pulse parameters in order to meet the design requirements. In particular, the transition width can be traded off against the inverted bandwidth—a matter not allowed by the conventional sech/tanh pulse. An efficient design algorithm is discussed and design examples are given to illustrate the effectiveness of the method in two extreme situations: (i) when a narrow transition bandwidth is required and (ii) when a wide band of frequencies is to be inverted in a short time. In both cases the superiority of the proposed method is demonstrated with respect to a conventional sech/tanh adiabatic pulse with similar parameters.

METHOD

For the sake of simplicity we limit our discussion to a specific trajectory, in particular the half-ellipse trajectory of the sin/cos and sech/tanh pulses. The modulation functions, after being parameterized by a function $\eta(t)$ of time, are given by

$$\omega_1(t) = A\cos(\eta(t)), \quad \eta\epsilon\left[-\frac{\pi}{2}, \frac{\pi}{2}\right]$$
$$\omega(t) = \omega_c - B\sin(\eta(t)), \qquad [4]$$

where $A = \omega_{1\max} = \gamma B_{1\max}$ is the nominal peak amplitude of the pulse. $B = \mathrm{SW}/2$, where SW is the inverted bandwidth and ω_c is the Larmor frequency of the slice center. The parameterizing function η varies between $-\pi/2$ and $\pi/2$ for an inversion pulse. Substituting this into Eq. [3] the adiabatic parameter in then given by

$$\Gamma(\Omega_0, t) = \frac{(v^2A^2\cos^2(\eta(t)) + (B\sin(\eta(t)) + \Omega_0)^2)^{3/2}}{|\dot\eta(t)vA(B + \Omega_0\sin(\eta(t)))|}, \qquad [5]$$

where $\Omega_0 = \omega_0 - \omega_c$ is the off-resonance frequency relative to the slice center.

Herein we are concerned with adiabatic pulses which invert M_z over a *wide band* of Larmor frequencies. Before the pulse is applied the magnetization is assumed to be at its equilibrium value M_0 in the z direction. For convenience, we work in units where $M_0 = 1$. Three regions can be recognized (*14*): (i) the in-slice region, $|\Omega_0| < \mathrm{SW}/2 - c_0$, where M_z is inverted; (ii) the out-of-slice region, $|\Omega_0| > \mathrm{SW}/2 + c_0$, where the equilibrium magnetization retains its initial value; and (iii) the transition region of width $2c_0$ in between, $\mathrm{SW}/2 - c_0 < |\Omega_0| < \mathrm{SW}/2 + c_0$, where the final magnetization varies between those two states. The adiabatic condition [2] must be fulfilled for all Larmor frequencies in the first two regions, but by definition, breaks down in the transition region in between (*14, 15*).

The adiabatic parameter Γ was seen in Eq. [5] to be a function of the off-resonance frequency Ω_0. The on-resonance results of Refs. (*6–8*) can be generalized to include wide-band adiabatic pulses by requiring that the pulse fulfill the adiabatic condition, viz.

$$\Gamma(\Omega_0, t) \ge \gamma_0, \qquad [6]$$

during the entire pulse duration $t \in [0, T]$, for off resonances Ω_0 within the in-slice and out-of-slice regions, and for a specified range of inhomogeneity $v_{\min} \le v \le v_{\max}$. The parameter γ_0 determines the lowest allowed value of the adiabatic parameter Γ. The shaded area in Fig. 1 defines the support region, designated Q, upon which we require condition [6] to be fulfilled. The value of the parameter c_0 affects the transition width of the resulting pulse. To a close approximation, $2c_0$ gives the transition width when γ_0 is set to its lowest value that still renders inversion.

Rearranging Eqs. [5] and [6] and assuming that η is an ascending function of t we can write

$$\dot\eta(t) = \frac{d\eta}{dt} \le \frac{1}{\gamma_0}\frac{(v^2A^2\cos^2(\eta) + (B\sin(\eta) + \Omega_0)^2)^{3/2}}{|vA(B + \Omega_0\sin(\eta))|} \equiv \frac{1}{\gamma_0} f(\eta; \Omega_0, v). \qquad [7]$$

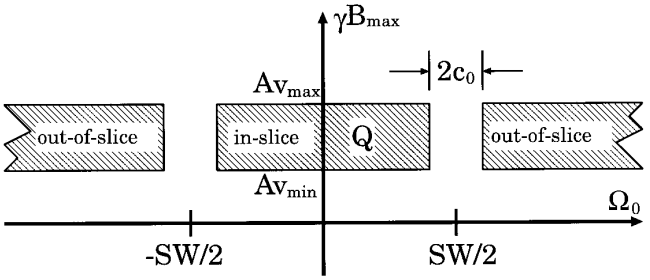

FIG. 1. Support region for inversion pulse upon which the adiabatic condition $\Gamma(\Omega_0, t) \geq \gamma_0$ is required to be fulfilled. The slice width is SW and the parameter c_0 affects the transition width of the resulting pulse. The range of RF inhomogeneity is $v_{\min} \leq v \leq v_{\max}$ so that the maximal peak RF amplitude varies between $Av_{\min}$ and $Av_{\max}$.

For a given value of η, the function f achieves a certain minimal value within the support area Q. We denote this minimal value of $f(\eta; \Omega_0, v)$ by $f_m(\eta)$. If $\dot{\eta}(t)$ at each η is set equal to this minimal value, then the condition required by Eq. [7] will be fulfilled upon the entire domain Q. Equating $\dot{\eta}(t)$ with $f_m(\eta)$ defines the time derivative of $\eta(t)$ as a function of η itself. This can be solved for t, by

$$t(\eta) = \gamma_0 \int_{-\pi/2}^{\eta} d\eta' [f_m(\eta')]^{-1}, \quad \eta \in \left[-\frac{\pi}{2}, \frac{\pi}{2}\right]. \qquad [8]$$

The total duration of the inversion pulse is then

$$T = \gamma_0 \int_{-\pi/2}^{\pi/2} d\eta' [f_m(\eta')]^{-1}.$$

Summarizing, the algorithm for designing wide-band pulses is:

1. We are given the desired inverted slice width $B = SW/2$ and the range of RF amplitudes $[Av_{\min}, Av_{\max}]$. The transition width parameter c_0 is chosen; as a first approximation, half the desired transition width may be used. These parameters define the support area Q.
2. Integrate the differential equation [8]. The result is the function $t(\eta)$. Here $f_m(\eta)$ denotes the minimal value that $f(\eta; \Omega_0, v)$ (Eq. [7]) obtains upon the support area Q for a given value of η.
3. Invert $t(\eta)$ to obtain $\eta(t)$.
4. The pulse modulation functions are determined by Eq. [4].

Several comments are in order. In Step 2 the differential equation [8] is integrated using numerical techniques (*16*) which require computation of the value of the integrand $f_m(\eta)$ for a given value of η. It is simplest to calculate f_m—the minimum of $f(\eta; \Omega_0, v)$ within the support area Q—by a direct search method or some other numerical algorithm. In general, this is difficult to perform analytically because of the irregular shape of the domain Q. In the next section we describe an efficient algorithm for calculating f_m.

The value of γ_0 in Eq. [8] determines the time scale of the pulse. In addition, it represents the minimal value of the adiabatic parameter within Q (cf. Eq. [6]). For simplicity, Step 2 can be performed for an arbitrary value of this parameter, say $\gamma_0 = 1$. The final pulse should then be tested by simulation for different time scales (representing different values of γ_0). The shortest pulse that can still render satisfactory inversion is finally selected. From our experience, the lowest value of γ_0 is $\gamma_0 \approx 4$.

The parameter c_0 controls the transition width. Reducing this parameter decreases the transition width; the pulse duration, however, will then increase. In practice, this value should be adjusted by experimentation, until both the transition and the pulse duration are satisfactory. Note that the trade-off between pulse parameters, which is characteristic of the method described here, is not possible in a conventional sech/tanh pulse where the transition width is inversely proportional to the slice duration and is solely determined by it (*17*). For a given pulse duration, if the slice width SW is made too large, the pulse will cease to invert. This point is exemplified under Results below.

Computation of f_m

Recall that $f_m(\eta)$ is the minimal value that $f(\eta; \Omega_0, v)$ achieves within the support area Q shown in Fig. 1. The simplest solution adopted by several authors (*10–13*) is to use an approximation by which the minimal value is obtained at resonance where $\omega_0 = \omega(t)$. It is now shown that the actual expression is more complicated, and by using the exact result we ensure that adiabaticity is indeed maintained across the entire inverted band. An efficient search method for numerically computing the minimal value throughout the irregularly shaped support Q is discussed.

For given values of η and v we can solve

$$\frac{\partial f(\eta; \Omega_0, v)}{\partial \Omega_0} = 0, \qquad [9]$$

for Ω_0. The solution is given by

$$\Omega_0^m(\eta, v) = -B\sin(\eta) + \frac{-3B\cos^2(\eta) + \sqrt{9B^2\cos^4(\eta) + 2v^2A^2\sin^2(2\eta)}}{4\sin(\eta)}. \qquad [10]$$

Ω_0^m is, then, the off resonance at which f is minimal for given values of η and υ. We are not, however, concerned with the entire range of off resonances; only the in-slice and out-of-slice regions are of interest to us. Therefore, if Ω_0^m falls within the transition region (i.e., $SW/2 - c_0 < |\Omega_0^m| < SW/2 + c_0$) it should be substituted by the lowest value that f achieves at one of the two adjacent boundaries. For example, if $SW/2 - c_0 < \Omega_0^m < SW/2 + c_0$, then the following two values should be computed:

$$f_1 = f(\eta; SW/2 - c_0, \upsilon)$$
$$f_2 = f(\eta; SW/2 + c_0, \upsilon).$$

If $f_1 < f_2$ then $\Omega_0^m = SW/2 - c_0$ is used, and vice versa, if $f_2 < f_1$ then $\Omega_0^m = SW/2 + c_0$ is used.

Using this method we can calculate $\Omega_0^m(\eta, \upsilon)$, which is the off resonance at which f is minimal for given values of η and υ. In order to find $f_m(\eta)$, all that is left to do is to calculate the minimal value of $f(\eta; \Omega_0^m(\eta, \upsilon), \upsilon)$ as a function of υ. For example, we may divide the range of $\upsilon_{min} \le \upsilon \le \upsilon_{max}$ into N sections with midpoints υ_i. For each υ_i, $\Omega_0^m(\eta, \upsilon_i)$ is computed as described above and then the value of $f(\eta; \Omega_0^m, \upsilon_i)$ is calculated. f_m is, thus, the lowest value of $f(\eta; \Omega_0^m(\eta, \upsilon_i), \upsilon_i)$ over all υ_i. Rather than conducting such a direct search over υ_i, more efficient one-dimensional minimum-finding algorithms can be employed (*16*). Note that the method used must require only evaluations of the *function* to be minimized (i.e., f) and not evaluations of its *derivatives*, because the derivative $\partial f(\eta; \Omega_0^m(\eta, \upsilon), \upsilon)/\partial\upsilon$ is not necessarily defined.

RESULTS

We now demonstrate the performance of the optimized pulse via two examples which examine two extreme cases: (i) a large bandwidth is to be inverted in a short time using low RF amplitude and (ii) a narrow transition is sought. In both cases the optimized pulse is compared with a conventional sech/tanh adiabatic pulse which is known to be an efficient and robust pulse.

The pulses described below were implemented on a Prestige 2T system (Elscint Ltd., Haifa, Israel), in order to provide experimental validation of the results obtained by simulation. The experimental setup was described in detail in Ref. (*14*).

Example 1: Large Inversion Band

The objective of our first example is to design a pulse which is capable of inverting a large bandwidth using a weak RF amplitude in a short time. It is shown that this can be achieved by sacrificing the transition width. We are trying to invert a bandwidth of $SW/2\pi = 8$ kHz with an RF amplitude as low as $A/2\pi = \gamma B_{1\,max}/2\pi = 0.8$ kHz. The computation of f_m was performed with a transition width parameter of $c_0/2\pi = 1.2$ kHz and over a range of RF inhomogeneity $0.8\text{ kHz} \le \upsilon A/2\pi \le 6$ kHz (these parameters determine the shape of the support area Q shown in Fig 1). We note that a slice width parameter $2B/2\pi = 9$ kHz (instead of 8 kHz) was used because the final result with this value corresponds better to the desired inverted bandwidth. Simulations were performed on the result of the optimization procedure to determine the lowest possible value of the adiabatic parameter γ_0 which is capable of rendering satisfactory inversion; the value chosen was $\gamma_0 = 2.95$ which yields a pulse of duration 9 ms. The amplitude and frequency modulation functions of the optimized RF pulse are plotted in Figs. 2a and 2b. Figure 2c displays the resulting computer-simulated slice profile. For comparison, the dashed line in the figure represents a conventional sech/tanh pulse with the same parameters (i.e., duration, slice width, and peak amplitude). It can be seen that the sech/tanh pulse does not achieve full inversion. Its transition, however, is sharper than the optimized pulse. Experimental validation of this pulse is depicted in Fig. 2d.

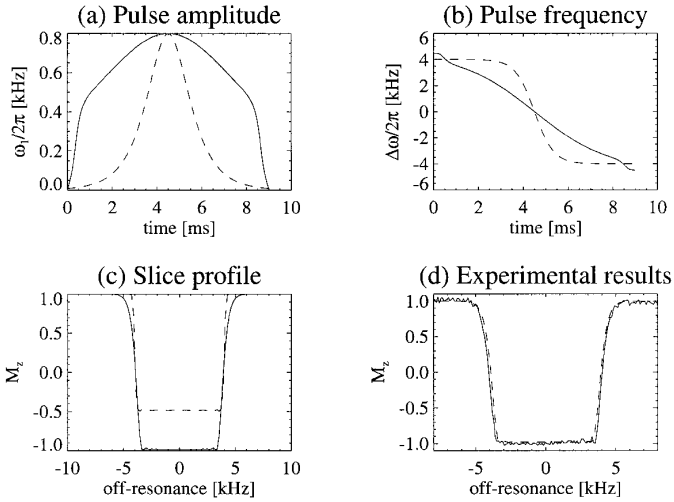

FIG. 2. Optimization of a pulse which is intended to invert a large bandwidth (8 kHz) using a weak RF amplitude (0.8 kHz) in a short time (9 ms). Pulse modulation functions (a) amplitude and (b) frequency, and (c) simulated slice profile of optimized pulse (solid line) and a conventional sech/tanh pulse (dashed line) with similar parameters. (d) Experimental result (solid line) compared with simulated result (dashed line) for optimized pulse. Parameters used for optimization: $2B/2\pi = 9$ kHz, transition width parameter $c_0/2\pi = 1.2$ kHz, range of RF inhomogeneity $0.8\text{ kHz} \le \upsilon A/2\pi \le 6$ kHz. Minimal value of adiabatic parameter $\gamma_0 = 2.95$ which yields a pulse duration of 9 ms. Parameters for sech/tanh adiabatic pulse: $SW/2\pi = 8$ kHz, $\gamma B_{1\,max}/2\pi = 0.8$ kHz.

The adiabatic behavior of the pulse is demonstrated by studying its sensitivity to inhomogeneity of the RF field. This is done by plotting contours of the longitudinal magnetization at the end of the pulse at each off-resonance frequency

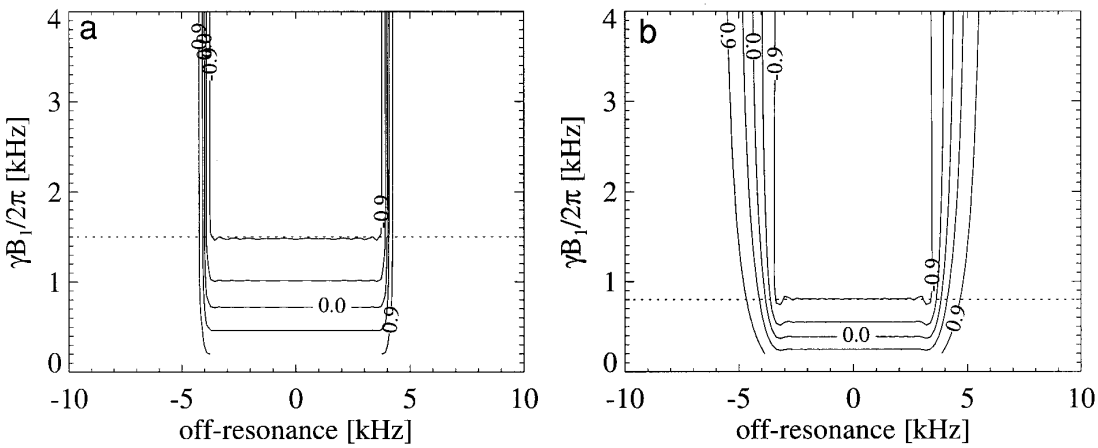

FIG. 3. Stability in the presence of RF field inhomogeneity: contours of the longitudinal magnetization at the end of the pulse at different RF amplitudes. (a) sech/tanh pulse and (b) optimized pulse (corresponding to the pulse in Fig. 2). The horizontal dotted lines designate the threshold RF amplitude above which inversion is ensured.

in the presence of field imperfections. In Fig. 3 these contours are plotted as a function of the maximal value of the applied RF field for the optimized pulse and the corresponding sech/tanh adiabatic pulse. For both pulses the slice profile is retained over a large variation in RF amplitude. However, full magnetization inversion is obtained for the new pulse at a much lower B_1 amplitude.

The adiabatic behavior of the pulse can further be demonstrated by examining its performance in two extreme situations. In the first, the *adiabaticity* is affected by varying the B_1 amplitude of the pulse. Figure 4 plots the z component of the final magnetization at the slice center (on resonance) as a function of the maximal B_1 amplitude applied during the pulse. It is seen that full inversion (defined herein as $M_z \leq -0.95$) is achieved when the maximal pulse amplitude is 0.8 kHz for the optimized pulse versus 1.5 kHz for the sech/tanh pulse. These conditions correspond to the horizontal dotted lines in Fig. 3.

In the second extreme case, the *efficiency* of the pulse is tested by examining its ability to invert the magnetization at short durations. Figure 5 plots the final M_z at the slice center for various pulse durations using the maximal B_1 amplitude of 0.8 kHz. It can be seen that the optimized pulse achieves full inversion (on resonance) for pulse durations as low as 9 ms whereas the sech/tanh pulse requires more than 30 ms to accomplish inversion.

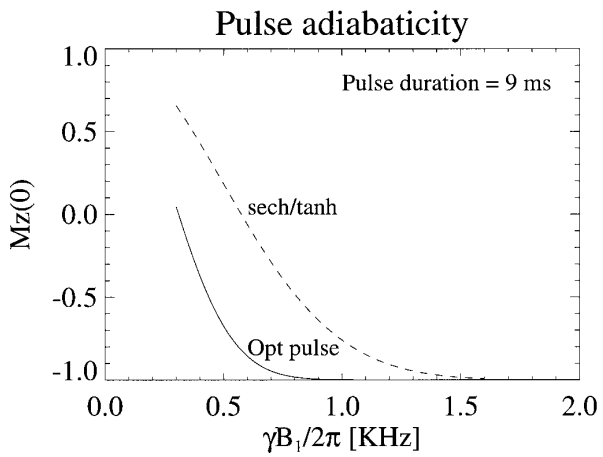

FIG. 4. The adiabatic performance of the optimized pulse of Fig. 2 compared with that of a sech/tanh pulse using the same parameters. The M_z component of the final magnetization at the slice center is plotted for various maximal RF amplitudes with a pulse duration of 9 ms. Inverted bandwidth is $\mathrm{SW}/2\pi = 8$ kHz.

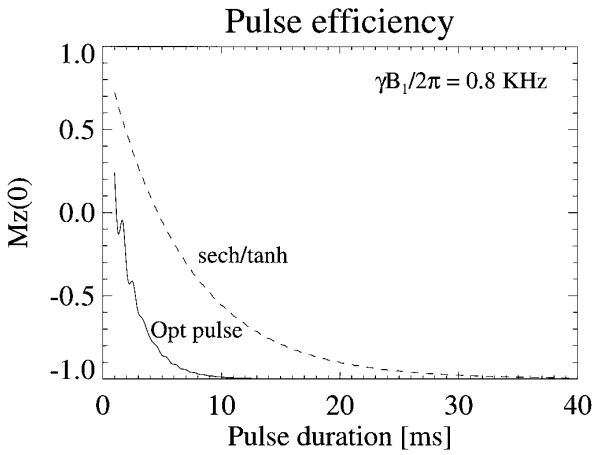

FIG. 5. Pulse efficiency: The M_z component of the final magnetization at the slice center is plotted for various pulse durations. The optimized pulse of Fig. 2 is compared with a sech/tanh pulse using the same parameters. Inverted bandwidth is $\mathrm{SW}/2\pi = 8$ kHz and the maximal RF amplitude is $\gamma B_{1\,\max}/2\pi = 0.8$ kHz.

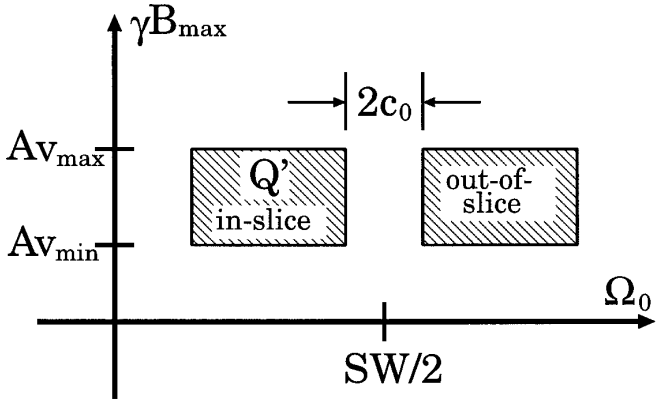

FIG. 6. Support region for a pulse which performs fat suppression by inversion. The adiabatic condition $\Gamma(\Omega_0, t) \geq \gamma_0$ is required to be fulfilled upon the shaded area. The parameter c_0 affects the transition width of the resulting pulse which is desired to be kept to a minimum. The range of RF inhomogeneity is $v_{\min} \leq v \leq v_{\max}$ so that the maximal peak RF amplitude varies between $Av_{\min}$ and $Av_{\max}$.

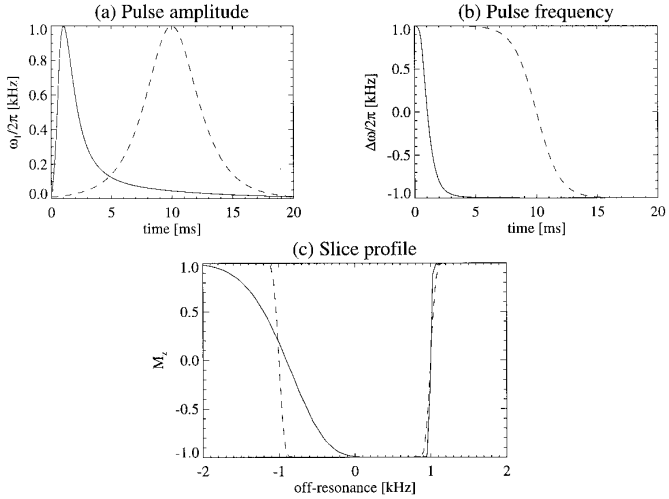

FIG. 7. Optimization of a pulse which is designed to perform fat suppression by inversion. Pulse modulation functions (a) amplitude and (b) frequency and (c) simulated slice profile of optimized pulse (solid line) and a conventional sech/tanh pulse (dashed line) with similar parameters. Parameters used for optimization: $2B/2\pi = 2$ kHz, transition width parameter $c_0/2\pi = 50$ Hz, range of RF inhomogeneity 1 kHz $\leq vA/2\pi \leq 4$ kHz. The interval of interest on both sides of the transition (cf. Fig. 6) is 0.5 kHz. Minimal value of adiabatic parameter $\gamma_0 = 5.35$ which yields a pulse duration of 20 ms. Parameters for sech/tanh adiabatic pulse: $\mathrm{SW}/2\pi = 2$ kHz, $\gamma B_{1\,\max}/2\pi = 1$ kHz.

Example 2: Sharp Transition

In our second example we attempt to design a pulse for performing fat suppression by inversion. The purpose is to invert the longitudinal magnetization for spins below a certain Larmor frequency while leaving it untouched for spins above that frequency. The main goal is to keep the transition region as narrow as possible because of the small chemical shift between the signals (~3.5 ppm). This process is described in detail in Ref. (*17*).

In this technique only a single transition of the inversion pulse is utilized. Moreover, the final magnetization is only significant upon a certain finite frequency band on either side of the transition. This bandwidth should contain the spectral region where substantial signal is emitted by the water and lipid protons. The symmetric bi-sided form of the support area Q shown in Fig. 1 may be replaced by the less restrictive single-sided shape Q' depicted in Fig. 6. Here the transition region of width $2c_0$ is enclosed by two frequency intervals: the inverted band on the left and the out-of-slice region, where the magnetization is left untouched, on the right.

The parameters used for the optimization were a bandwidth of $2B/2\pi = \mathrm{SW}/2\pi = 2$ kHz, transition width parameter of $c_0/2\pi = 50$ Hz, and range of RF inhomogeneity 1 kHz $\leq vA/2\pi \leq 4$ kHz. The bandwidth on both sides of the transition (cf. Fig. 6) is 0.5 kHz. The lowest adiabatic parameter chosen was $\gamma_0 = 5.35$ which yields a pulse of duration 20 ms.

The amplitude and frequency modulation functions of the optimized RF pulse are plotted in Figs. 7a and 7b. Figure 7c displays the resulting (computer-simulated) slice profile. The dashed line in the figure represents a corresponding sech/tanh pulse. The asymmetric nature of both the modulation functions and the frequency response is clearly visible. A single transition has, indeed, been sharpened at the expense of the other transition which is immaterial to our purpose. The extent of this improvement is exhibited in Fig. 8 which compares the optimized transition to that of the sech/tanh pulse; this figure is a detail of Fig. 7c. Comparing the transition bandwidth of both pulses in the range where M_z switches between ± 0.95 (horizontal dotted lines in the figure), it is concluded that the transition has been reduced by a factor of 77 Hz/195 Hz ≈ 0.4.

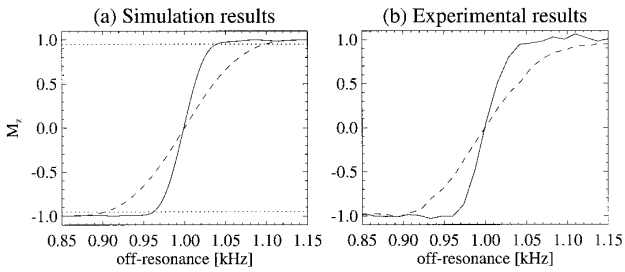

FIG. 8. Transition region of the optimized pulse of Fig. 7 (solid line) compared with that of an equivalent sech/tanh pulse (dashed line). (a) Simulated results and (b) experimental results.

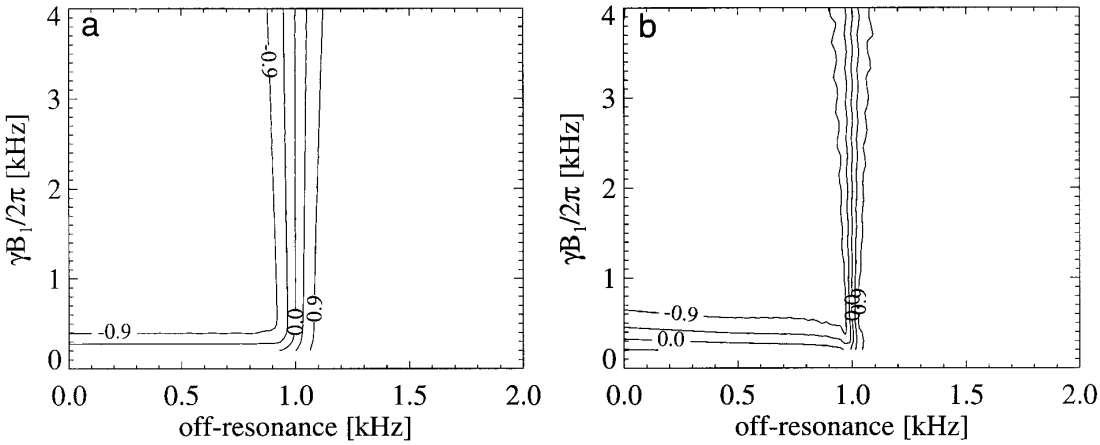

FIG. 9. Stability in the presence of RF field inhomogeneity: contours of the longitudinal magnetization at the end of the pulse at different RF amplitudes. (a) sech/tanh pulse and (b) optimized pulse (corresponding to the pulse in Fig. 7).

Figure 9 displays stability plots of both pulses. It can be seen that the optimized pulse is very robust as its sharpness is maintained over a large range of amplitudes.

DISCUSSION

Adiabatic pulses are capable of providing robust and reliable magnetization inversion which grants them an important role as inversion pulses in many MRI applications. Inhomogeneity of the RF field occurs frequently in magnetic resonance imaging due to magnetic loading of the patient's body (*18–20*). RF coils contribute to the field inhomogeneity both due to constraints imposed by coil design (*21*) and in the case of the RF field of a surface coil which declines as the distance from the coil center increases. Therefore, it is essential to design pulses which are insensitive to RF field inhomogeneity.

As the static magnetic field increases, the RF power dissipation in the patient's body increases dramatically (*22*). This has the effect of reducing the maximum available B_1 amplitude because much more RF power is required. In addition, maximal RF amplitude is a limitation of the equipment being used, in particular, the RF power amplifier.

In many applications the duration of the adiabatic pulse is a significant consideration. This duration is limited due to T_2 decay so that the largest pulse duration must be much less than the shortest T_2 that is being examined. Another constraint is imposed by the pulse sequence being used. For example, in inversion-recovery sequences a shorter inversion pulse would enable one to image more slices simultaneously. Consequently, it is important to design efficient adiabatic pulses that invert M_z at the shortest possible time.

Adiabatic pulses are capable of alleviating the above-mentioned difficulties by enabling one to design pulses which are insensitive to RF field inhomogeneity, and can invert M_z over a large frequency bandwidth using low B_1 levels at a short duration. These qualities derive from two important properties of adiabatic pulses: First, an important advantage of such pulses over conventional 180° pulses is that the inversion of the longitudinal magnetization (and the slice profile) is retained for any RF field strength above a given threshold of B_1 amplitude. Therefore, a robust magnetization inversion is ensured even if the magnetic field is very inhomogeneous provided that the weakest field exceeds this threshold amplitude. This property is demonstrated both by Fig. 4 and by the stability plots in Figs. 3 (i.e., inversion is ensured above the horizontal dotted line) and 9.

Second, adiabatic pulses are capable of inverting a large frequency bandwidth using a small RF amplitude. The inversion can be achieved provided that the pulse duration is long enough so that the adiabatic condition is fulfilled. In contrast, for conventional 180° pulses, the maximum inverted bandwidth is less than twice the maximum available B_1 amplitude (in frequency units). This point is illustrated in Fig. 5 where it is seen that inversion is ensured above a certain duration.

Because of their advantages adiabatic pulses produce a robust and reliable magnetization inversion and are, therefore, extensively used in a wide variety of imaging applications, for example, inversion-recovery sequences, MP-RAGE, MR angiography, and ''black-blood'' imaging.

The method described herein starts off by defining the support area which determines the ranges of both off resonances and RF inhomogeneity factors where the pulse is required to perform well. The time spent sweeping each point along the half-ellipse trajectory is then determined so that the adiabatic condition $\Gamma(\Omega_0, t) \geq \gamma_0$ is fulfilled with respect to every point in the support area. This is achieved

by first finding the point within the support area for which the adiabatic parameter Γ is the lowest, and then forcing the equality $\Gamma = \gamma_0$ for this point. Finally, the precise value of γ_0 is determined by simulation; the lowest value that can still render satisfactory inversion is selected.

The lowest value of the adiabatic parameter, γ_0, must be determined experimentally. It was mentioned above that this value is approximately $\gamma_0 \approx 4$. In our examples we obtained a lower value (2.95) when trying to invert a large bandwidth and a higher value (5.35) when sharpening the transition. This trend was confirmed by other experiments we performed as well.

As mentioned above, the parameter c_0 controls the transition width. Reducing this parameter decreases the transition width; the pulse duration, however, will then increase. In practice, this value should be adjusted by experimentation until both the transition width and the pulse duration are satisfactory. It is interesting to note that to a close approximation, $2c_0$ gives the transition width when γ_0 is set to the lowest value that still enables inversion. This is confirmed by both our examples (cf. Figs. 2c and 8).

The conventional sech/tanh adiabatic pulse and the optimized pulse both trace the identical half-ellipse trajectory and do so at the same duration. The *sweep rate,* however, is different: it was adjusted in the optimized pulse to achieve the goal of larger inversion band in the first example and a sharper transition in the second. How is this accomplished? In the sech/tanh pulse the transition width is determined exclusively by the pulse duration (*17, 23*). This effect is demonstrated in Fig. 2c which shows that the sech/tanh pulse maintains its sharp transition though it could not reach an inversion. The optimization process allows us to trade off the transition sharpness against the inverted bandwidth; one may be sacrificed in favor of the other. This is precisely what happened in both our examples. In the first example the transition width was sacrificed in order to obtain a larger inverted bandwidth. In the second example the transition is narrow, although a smaller frequency band is inverted.

It is interesting to note that for a given set of parameters we could, in our experiments, find a unique value of c_0 which yields a pulse almost identical to the sech/tanh adiabatic pulse. This value reflects the specific trade-off between transition sharpness and inverted bandwidth which distinguishes the sech/tanh pulse. It also serves to explain the robust behavior of the sech/tanh pulse. In the Appendix, an approach based on the adiabatic condition, similar to the one described herein, is used to explain the adiabaticity of the sech/tanh pulse.

In medical imaging applications, especially in high-field systems, the specific absorption rate (SAR) is an important specification of an RF pulse. The SAR measures the amount of RF energy dissipated by the patient's body per unit time. The RF energy of a pulse with duration T is proportional to

$$E_{\text{pulse}} \propto \int_0^T (\gamma B_1(t))^2 dt.$$

The SAR induced by the pulse depends on the number of times per second that this pulse is employed. For Example 1 we compare the energy of the optimized pulse with parameters as shown in Fig. 2 ($T = 9$ ms, $\gamma B_{1\,\max}/2\pi = 0.8$ kHz) with a sech/tanh pulse of equal duration, but with a higher peak RF amplitude ($\gamma B_{1\,\max}/2\pi = 1.5$ kHz) which ensures inversion (cf. horizontal dotted lines in Fig. 3). We then obtain

$$\text{Example 1:} \qquad \frac{E_{\text{new pulse}}}{E_{\text{sech/tanh}}} = 93\%.$$

We conclude that in order to invert adiabatically an 8-kHz bandwidth in 9 ms, not only does the optimized pulse allow us to use only 53% of the maximal RF amplitude, but it performs the task while dissipating less energy than a sech/tanh pulse.

As for Example 2, the energy ratio is compared for the same parameters that are displayed in Fig. 7,

$$\text{Example 2:} \qquad \frac{E_{\text{new pulse}}}{E_{\text{sech/tanh}}} = 37\%,$$

which exhibits an even larger decrease in energy.

In this paper we used the conventional half-ellipse trajectory throughout. It is straightforward to apply the optimization technique described herein to other types of trajectories. In particular, we tested a parametric family of trajectories which we call $\sin^\alpha/\cos^\alpha$ (cf. Eq. [4]):

$$\omega_1(t) = A \cos^\alpha(\eta(t)), \quad \eta \in \left[-\frac{\pi}{2}, \frac{\pi}{2}\right]$$

$$\omega(t) = \omega_c - B \operatorname{sign}(\eta(t))|\sin(\eta(t))|^\alpha. \qquad [11]$$

The parameter α determines the convexity of the trajectory: $\alpha = 1$ yields the regular half-ellipse trajectory, whereas for lower values of α one obtains a more bulging trajectory. We performed optimizations with the parameters of Example 2 where we tested the sharpness of the transition as a function of the convexity parameter α. The results show that for $\alpha = 0.465$ the transition width can be reduced by an additional 4% with respect to the original results of Example 2 (acquired for $\alpha = 1$). The reduced transition was accompanied by a SAR increase of 17%. Note that a similar inflated trajectory was proposed by us in a previous publication (*14*)

where it was derived analytically. There, too, a similar increase in SAR was obtained.

CONCLUSIONS

In this paper a method is described by which optimized modulation functions can be constructed to render insensitivity to B_1 inhomogeneity over a predetermined B_1 range and over a wide band of frequencies. This is accomplished by requiring that the optimized pulse fulfill the adiabatic condition over the range of B_1 inhomogeneity and over the desired frequency band for the complete duration of the pulse. The slice profile is improved by optimizing the rate of motion along the given half-ellipse trajectory.

It was shown that the optimized pulse can be tailored to the specific design requirements; in particular, the transition sharpness may be traded off against the inverted bandwidth. In both cases the superiority of the new pulse with respect to a conventional sech/tanh adiabatic pulse was established. This follows from the fact that the sech/tanh pulse exhibits a *particular* relationship between its transition sharpness and its inverted bandwidth; the optimization, on the other hand, allows one to meet the specific requirements at hand.

APPENDIX

Derivation of the sech/tanh Pulse from the Adiabatic Condition

It is shown that, using a process similar to the one described in this paper, we can analytically derive expressions for the sech/tanh pulse. We begin with Eq. [7] (for $v = 1$):

$$\dot{\eta}(t) \leq \frac{1}{\gamma_0} \frac{(A^2\cos^2(\eta) + (B\sin(\eta) + \Omega_0)^2)^{3/2}}{|A(B + \Omega_0\sin(\eta))|}. \quad [A1]$$

Assuming that the minimum value of $\dot{\eta}$ with respect to Ω_0 is obtained inside the inverted band, i.e., $|\Omega_0| \leq B$, then with regard to the denominator of Eq. [A1] it follows that $|B + \Omega_0\sin(\eta)| \leq 2B$. A more conservative inequality for $\dot{\eta}$ is, therefore,

$$\dot{\eta}(t) \leq \frac{1}{\gamma_0} \frac{(A^2\cos^2(\eta) + (B\sin(\eta) + \Omega_0)^2)^{3/2}}{2AB}. \quad [A2]$$

It is easy to see that the minimal value of the right-hand side of Eq. [A2] is obtained for

$$\Omega_0^{\mathrm{m}}(\eta) = -B\sin(\eta). \quad [A3]$$

The physical interpretation of Eq. [A3] is that the minimal value of the adiabatic parameter is obtained at resonance where $\omega_0 = \omega(t)$ (cf. Eq. [4]). It is also illuminating to compare Eq. [A3] with Eq. [10]. These two equations differ by the rightmost term in Eq. [10] which is comparatively small in most practical cases. In particular, for negative (positive) values of η the actual Ω_0^{m} (in Eq. [10]) is lower (higher) than the synthesizer frequency.

Substituting Eq. [A3] into Eq. [A2] and requiring equality yields the following equation for $\dot{\eta}$:

$$\frac{d\eta}{dt} = \frac{1}{\gamma_0}\frac{A^2}{B}\cos(\eta).$$

This simple equation can be analytically integrated as was done in Eq. [8] and an expression for $t(\eta)$ obtained. Inverting the latter we get

$$\eta(t) = 2\arctan\left(\tanh\left(\frac{1}{2}\frac{A^2}{B}\frac{t}{\gamma_0}\right)\right).$$

Substituting this expression into Eq. [4] and using some well-known trigonometric identities we obtain

$$\omega_1(t) = A\,\mathrm{sech}(\beta t)$$
$$\omega(t) = \omega_c - B\tanh(\beta t),$$

where

$$\beta = \frac{1}{\gamma_0}\frac{A^2}{B},$$

which are precisely the equations for the sech/tanh adiabatic pulse.

Summarizing, the sech/tanh pulse is a particular case of our method of optimization if we assume that the minimal value of f is obtained at the Larmor frequency of the synthesizer. On the one hand, when this assumption is fulfilled, the sech/tanh is optimal; on the other hand, when it breaks down, the optimization method presented herein yields better results. Our design examples demonstrate this point for two extreme cases where the approximation fails.

REFERENCES

1. K. Ugurbil, M. Garwood, A. R. Rath, and M. R. Bendall, *J. Magn. Reson.* **78,** 472 (1988).
2. C. P. Slichter, ''Principles of Magnetic Resonance,'' 3rd ed., Springer-Verlag, Berlin (1992).
3. C. J. Hardy, W. A. Edelstein, and D. Vatis, *J. Magn. Reson.* **66,** 470 (1986).

4. M. S. Silver, R. I. Joseph, and D. I. Hoult, *J. Magn. Reson.* **59,** 347 (1984).
5. M. R. Bendall and D. T. Pegg, *J. Magn. Reson.* **67,** 376 (1986).
6. K. Ugurbil, M. Garwood, and A. R. Rath, *J. Magn. Reson.* **80,** 448 (1988).
7. G. Town and D. Rosenfeld, *J. Magn. Reson.* **89,** 170 (1990).
8. T. E. Skinner and P.-M. L. Robitaille, *J. Magn. Reson.* **98,** 14 (1992).
9. A. J. Johnson, K. Ugurbil, and M. Garwood, Abstracts of the Society of Magnetic Resonance in Medicine, 8th Annual Meeting, Amsterdam, The Netherlands, p. 24 (1989).
10. Ē. Kupče and R. Freeman, *J. Magn. Reson. A* **115,** 273 (1995).
11. Ē. Kupče and R. Freeman, *J. Magn. Reson. A* **117,** 246 (1995).
12. Ē. Kupče and R. Freeman, *J. Magn. Reson. A* **118,** 299 (1996).
13. A. Tannús and M. Garwood, *J. Magn. Reson. A* **120,** 133 (1996).
14. D. Rosenfeld and Y. Zur, *Magn. Reson. Med.* **36,** 124 (1996).
15. S. Conolly, D. Nishimura, and A. Macovski, *J. Magn. Reson.* **83,** 549 (1989).
16. W. H. Press, S. A. Teukolsky, W. T. Vetterling, and B. P. Flannery, ''Numerical Recipes in C,'' 2nd ed., Cambridge Univ. Press, Cambridge (1992).
17. D. Rosenfeld, S. L. Panfil, and Y. Zur, *Magn. Reson. Med.* **37,** 793 (1997).
18. G. H. Glover *et al., J. Magn. Reson.* **64,** 255 (1985).
19. P. S. Tofts, *J. Magn. Reson. B* **104,** 143 (1994).
20. T. K. F. Foo, C. E. Hayes, and Y. Kang, *Magn. Reson. Med.* **23,** 287 (1992).
21. Y. Zur, U. Gotshal, and Y. Grach, Abstracts of the Society of Magnetic Resonance in Medicine, 11th Annual Meeting, Berlin, Germany, p. 271 (1992).
22. D. I. Hoult, C. Chen, and V. J. Sank, *Magn. Reson. Med.* **3,** 730 (1986).
23. D. Rosenfeld, S. L. Panfil, and Y. Zur, *J. Magn. Reson.* **126,** 221 (1997).